

Hadron production in e^+e^- annihilations at *BABAR*, and implications for the muon anomalous magnetic moment.

David R. Muller* for the *BABAR* Collaboration

SLAC National Accelerator Laboratory

E-mail: muller@slac.stanford.edu

The *BABAR* collaboration has an intensive program of studying hadronic cross sections in low-energy e^+e^- collisions, accessible at *BABAR* via initial-state radiation. Our measurements allow significant improvements in the precision of the predicted value of the muon anomalous magnetic moment. These improvements are necessary for shedding light on the current $\sim 3.5\sigma$ difference between the predicted and experimental values. We have published results on a number of processes with two to six hadrons in the final state. We report here the results of recent studies of the processes $e^+e^- \rightarrow K^+K^-$ and $e^+e^- \rightarrow 4$ hadrons, which constitute the main contribution to the hadronic cross section in the energy region between 1 and 3 GeV.

*XXI International Workshop on Deep-Inelastic Scattering and Related Subject -DIS2013,
22-26 April 2013
Marseilles, France*

*Speaker.

1. Introduction

We present results of several studies of electron-positron annihilations into exclusive final states using the tagged initial-state radiation (ISR) technique at BABAR, and discuss their impact on the theoretical prediction for the anomalous magnetic moment of the muon, $g_\mu - 2$. These include a new measurement of the $e^+e^- \rightarrow K^+K^-$ process [1], updated results with our full data sample on the $K^+K^-\pi^+\pi^-$ and $K^+K^-\pi^0\pi^0$ [2], and $\pi^+\pi^-\pi^+\pi^-$ [3] final states, and a preliminary result on the $\pi^+\pi^-\pi^0\pi^0$ final state. An updated measurement of the $p\bar{p}$ final state is presented separately.

The BABAR experiment [4] recorded e^+e^- data at center-of-mass (CM) energies near 10.6 GeV. However, the initial e^+ or e^- sometimes emits an energetic, real photon, denoted γ_{ISR} , before annihilating at a reduced CM energy, and the cross section for a process such as $e^+e^- \rightarrow \gamma_{\text{ISR}}K^+K^-$ can be related to the $e^+e^- \rightarrow K^+K^-$ cross section at the reduced energy by a well known radiator function. Using ISR events, one can therefore measure the reduced-energy process over a wide energy range in a single experiment.

Most ISR photons are emitted at small angles with respect to the e^\pm beams and escape detection, but 10% are emitted within the acceptance of the BABAR calorimeter and can be reconstructed. If such a “tagged” photon is sufficiently energetic, then the hadronic system is also well contained in the detector and is boosted toward it, resulting in full angular acceptance and good resolution for energies all the way down to threshold.

2. The $K^+K^-\pi^+\pi^-$, $K^+K^-\pi^0\pi^0$, $\pi^+\pi^-\pi^+\pi^-$ and $\pi^+\pi^-\pi^0\pi^0$ final states

We select $e^+e^- \rightarrow \gamma_{\text{ISR}}4$ -meson events by requiring at least one reconstructed photon candidate with energy above 3 GeV in the CM frame, reconstructing the four-meson system fully, and applying selection criteria to reduce backgrounds and improve resolution. Charged tracks are required to be reconstructed well within the acceptance of the tracking and particle identification systems, to be identified as pions or kaons in those systems, and not to be identified as electrons or muons in the calorimeters. We construct π^0 candidates from pairs of energy deposits in the calorimeter, and select high-quality candidates with invariant mass near the nominal π^0 mass. For each final state, we consider all combinations of appropriately identified particles and perform a set of kinematic fits under various hypotheses. We require the $\chi^2 < 30$ for the signal hypothesis, and reject combinations with a good χ^2 for some background hypotheses.

Backgrounds from other ISR processes with similar topology are evaluated from our previous or concurrent measurements, and most tracking and particle (mis)identification efficiencies are measured from the data. The dominant background at high energies is from the non-ISR process $e^+e^- \rightarrow \pi^04$ -mesons, in which an energetic π^0 is mistaken for a γ_{ISR} . We evaluate this background from the data by combining the γ_{ISR} candidate with other photon candidates in the event and measuring the size of the π^0 peak. This background generally amounts to a few percent near threshold, but then grows with increasing energy, eventually limiting the range of the measurement. Other backgrounds are evaluated from simulation and χ^2 control regions, and found to be small. We subtract the total estimated backgrounds bin by bin in each case.

The invariant mass distributions for the selected events are divided by the reconstruction efficiency and effective ISR luminosity to obtain cross sections for each process as a function of

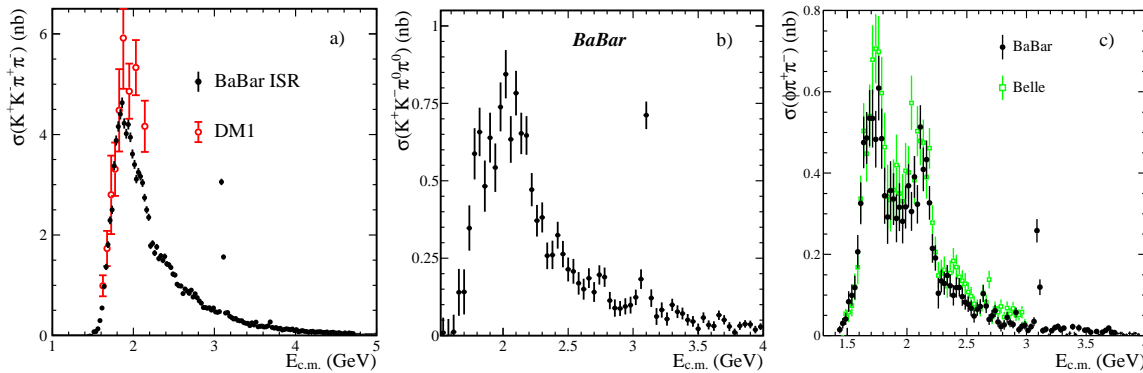


Figure 1: The (a) $K^+K^-\pi^+\pi^-$, (b) $K^+K^-\pi^0\pi^0$ and (c) $\phi\pi^+\pi^-$ cross sections as a function of energy. Also shown are all other measurements.

E_{CM} , the reduced CM energy. The $e^+e^- \rightarrow K^+K^-\pi^+\pi^-$ and $e^+e^- \rightarrow K^+K^-\pi^0\pi^0$ cross sections are shown in Figs. 1a and 1b, respectively. Only statistical errors are shown. The point-to-point systematic uncertainties are very small, but there are overall relative systematic uncertainties of 5% and 7%. Our $K^+K^-\pi^+\pi^-$ cross section is far more precise than the only previous measurement, and ours remains the only measurement of the $K^+K^-\pi^0\pi^0$ final state. Signals for the J/ψ and $\psi(2S)$ are evident, and there are signs of additional structure at lower E_{CM} . There is also considerable substructure: we measure separate cross sections for the sub-processes $e^+e^- \rightarrow K^*(890)K\pi$, $K_2^*(1430)K\pi$, $K^+K^-\rho^0(770)$ and $\phi(1020)\pi\pi$, and we observe contributions from the $K^*(890)\bar{K}^*(890)$, $K^*(890)\bar{K}_2^*(1430)$ and $K_1(1270)K$ final states.

The $\phi(1020)\pi^+\pi^-$ cross section is shown in Fig. 1c, along with a recent result from Belle. The peak near threshold corresponds to the $\phi(1680)$, and the second peak to a new particle, the $Y(2175)$, that we reported previously and has since been confirmed by BES and Belle. It decays predominantly to $\phi f_0(980)$; fitting the cross sections for $\phi\pi^+\pi^-$, $\phi\pi^0\pi^0$ and their ϕf_0 subsets simultaneously results in a 9.3σ observation of this state and improved measurements of its mass and width, $m_Y = 2180 \pm 8(\text{stat.}) \pm 8(\text{syst.}) \text{ MeV}/c^2$, $\Gamma_Y = 77 \pm 15(\text{stat.}) \pm 15(\text{stat.}) \text{ MeV}$.

The $e^+e^- \rightarrow \pi^+\pi^-\pi^+\pi^-$ cross section is shown in Fig. 2a, along with all previous results, including our previous measurement using half the data sample. Our results have shifted slightly, well within the systematic uncertainty, which is reduced to 2.5% in the peak region and by a large factor near threshold. We are consistent with all previous measurements, more precise than most, and have by far the widest coverage, with the only measurement above 2.2 GeV. The cross section shows a prominent peak populated mostly by the $a_1(1260)\pi$ submode and a second peak with a large contribution from $f_0(1370)\rho^0$. Other substructure is probably present, but a partial wave analysis is needed to disentangle all the components.

The $e^+e^- \rightarrow \pi^+\pi^-\pi^0\pi^0$ cross section is shown in Fig. 2b, and is compared with previous results over their range in Fig. 2c. We are consistent with all previous measurements within the systematic uncertainties, more precise than most, and have by far the widest coverage, with the only measurement above 2.2 GeV. There is considerably more structure and substructure than in the $\pi^+\pi^-\pi^+\pi^-$ cross section. We observe large contributions from the $\omega\pi^0$ and $a_1(1260)\pi$ submodes, as well as strong signals from $\rho^+\rho^-$ and $f_0(980)\rho^0$. Again, a partial wave analysis, preferably coupled to the $\pi^+\pi^-\pi^+\pi^-$ channel, is needed to disentangle all the components.

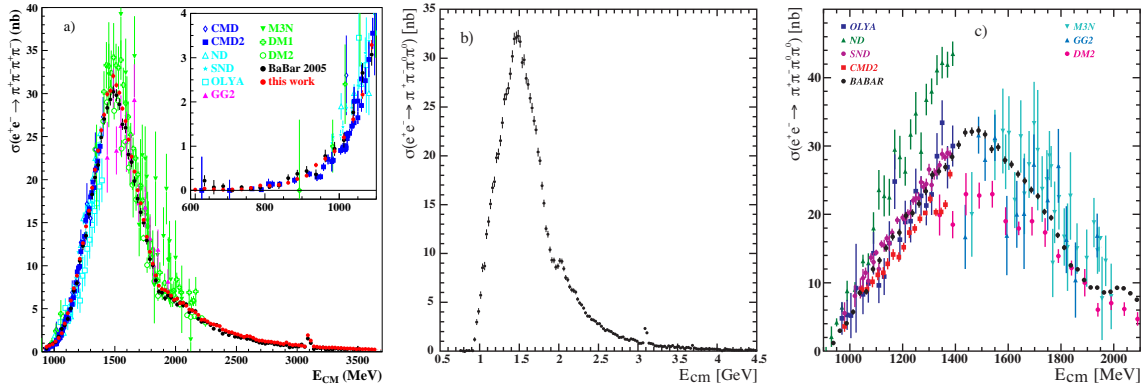


Figure 2: The (a) $\pi^+\pi^-\pi^+\pi^-$ and (b and c) $\pi^+\pi^-\pi^0\pi^0$ cross sections as a function of energy. Also shown are all previous measurements.

3. The K^+K^- final state

The $e^+e^- \rightarrow K^+K^-$ analysis is more complicated and aims for higher precision. It was done in parallel with our measurement of the $\pi^+\pi^-$ cross section [5], but some corrections specific to kaons are needed. We require an energetic γ_{ISR} candidate and two oppositely charged tracks both well within the detector acceptance and identified as K^\pm . We include the effects of higher-order ISR as well as final-state radiation (FSR), by performing pairs of kinematic fits: we first assume an additional undetected ISR photon along the beamline in an “ISR” fit; then we include each additional photon candidate in the event in an “FSR” fit (even though some of these could be ISR), and consider the one giving the best χ_{FSR}^2 . We then define signal and background regions in the two-dimensional space of $(\chi_{\text{ISR}}^2, \chi_{\text{FSR}}^2)$.

The backgrounds from $\gamma_{\text{ISR}}\pi^+\pi^-$ and $\gamma_{\text{ISR}}\mu^+\mu^-$ events are cross-calibrated in the data, along with the particle (mis)identification efficiencies, using the three event types and the $(\chi_{\text{ISR}}^2, \chi_{\text{FSR}}^2)$ distributions for different hypotheses. The $\pi^+\pi^-$ background is small except for the reflection of the ρ meson, where it reaches 20%. The $\mu^+\mu^-$ background is small at low E_{CM} , but limits the range of the measurement at high E_{CM} . Backgrounds from other ISR channels and from $e^+e^- \rightarrow K^+K^-\pi^0$ are evaluated as described above.

Every component of the detection efficiency is studied in detail and measured where possible from the data. This includes cross calibrating a number of overlapping triggers, and measuring the track finding efficiency and its correlations due to inefficient detector regions and proximity of the two tracks. Checks and corrections specific to charged kaons include those for the different rates of FSR, interactions in the detector material and decays in flight.

The $e^+e^- \rightarrow K^+K^-$ cross section is shown in Fig. 3 in several energy ranges. There is a prominent peak from the ϕ meson, and substantial structure in the 1.5-2.5 GeV range. Contributions from the J/ψ and $\psi(2S)$ are observed, measured and removed from these plots. The systematic uncertainty is 0.7% at the ϕ peak, and increases gradually to 3.4% at 1.4 GeV and 7% at 3 GeV.

Our measurements are consistent with most previous results, although the SND data are below (above) ours for $E_{\text{CM}} < (>)1.1$ GeV. We span the full range from threshold to 5 GeV, have the only measurement in the 2.1–3.6 GeV range, and are more precise than all but the three CLEO

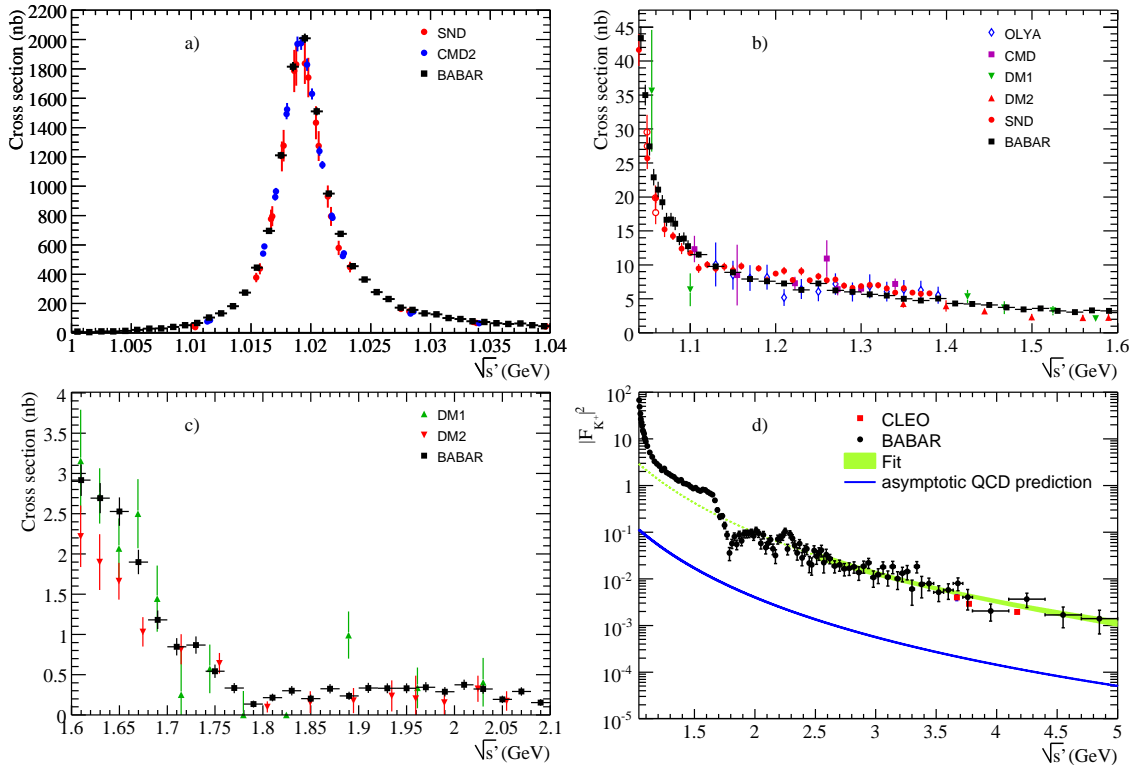


Figure 3: The $e^+e^- \rightarrow K^+K^-$ cross section as a function of energy over different ranges: (a) near the ϕ , 1.00–1.04 GeV; (b) from 1.04–1.6 GeV; (c) from 1.6–2.1 GeV; (d) over our full range from threshold to 5 GeV. All previous measurements are shown on (a–c) and the measurements from CLEO are shown on (d). The band on (d) represents the result of the fit described in the text, while the line indicates the asymptotic QCD prediction.

points near 4 GeV.

We perform a fit to the $e^+e^- \rightarrow K^+K^-$ cross section to extract the ϕ resonance parameters. The fit includes terms for several additional resonances, known and postulated, in order to assess their influence on the ϕ parameters and to describe the cross section over a wide range. We obtain a good description of the data from threshold up to 3 GeV, find that the ρ^0 and ω resonances have small but important effects, and that no additional resonances have any influence. We measure

$$m_\phi = 1019.51 \pm 0.02(\text{stat.}) \pm 0.05(\text{syst.}) \text{ MeV}/c^2 \quad \text{and} \quad \Gamma_\phi = 4.29 \pm 0.04(\text{stat.}) \pm 0.06(\text{stat.}) \text{ MeV},$$

where the first error is statistical and the second systematic. These results are consistent with the current world averages [6] and competitive with the best previous results. Useful measurements for any other resonances will require a coupled channel analysis.

We test the asymptotic prediction of QCD by fitting our data above 2.5 GeV with the function $f(s) = A\alpha_s^2(s)/s^n$, where A and n are free parameters. The fit result is shown as the band on Fig. 3d, and is consistent with all data above 2.5 GeV, as well as with much of the lower- s data. The fitted value of n is consistent with the predicted value of 2, but the value of A is a factor of four higher than the QCD prediction, which is shown as the line on Fig. 3d.

4. Results and conclusions

In summary, we continue our program at *BABAR* of measuring cross sections for as many exclusive final states as possible in e^+e^- annihilations at low CM energies. Here we show a new result on the K^+K^- final state, updated results on the $\pi^+\pi^-\pi^+\pi^-$, $K^+K^-\pi^+\pi^-$ and $K^+K^-\pi^0\pi^0$ final states, and a preliminary result on the $\pi^+\pi^-\pi^0\pi^0$ final state. In each case we measure the total cross section from threshold to 4.5 or 5 GeV, study any substructure, and extract J/ψ and $\psi(2S)$ branching fractions. In the $K^+K^-\pi^+\pi^-$ and $K^+K^-\pi^0\pi^0$ modes, we confirm the existence of a new state, the $Y(2175)$, which decays predominantly to $\phi f_0(980)$. In the K^+K^- final state we make competitive measurements of the parameters of the $\phi(1020)$ meson, and test the asymptotic prediction of QCD, which is found to be well below the data in the 2.5–5 GeV range.

Our cross section measurements are consistent with most previous results, cover wider ranges, and are generally more precise. They can be used to improve the calculation of the hadronic contribution to the anomalous magnetic moment of the muon $a_\mu = g_\mu - 2$, and shed light on the current discrepancy of $(28.7 \pm 8.0) \times 10^{-10}$ between the experimental and theoretical values. It is conventional to quote contributions integrated from threshold up to 1.8 GeV, and for our $\pi^+\pi^-\pi^+\pi^-$ and K^+K^- modes, we calculate

$$\begin{aligned} a_\mu^{4\pi} &= (13.64 \pm 0.03(\text{stat.}) \pm 0.36(\text{syst.})) \times 10^{-10} \quad \text{and} \\ a_\mu^{KK} &= (22.93 \pm 0.18(\text{stat.}) \pm 0.22(\text{syst.})) \times 10^{-10}. \end{aligned}$$

The former represents a 32% improvement over the current average (which includes our previous result), and the latter is the first measurement over this full range and a factor of 2.6 more precise than the current average. Along with the $\pi^+\pi^-\pi^0\pi^0$ mode, on which we expect to achieve a $\sim 5\%$ relative uncertainty, these are the dominant modes in the 1–2 GeV region.

Our measured contributions are consistent with previous averages, so they do not resolve the discrepancy between theory and experiment, but do exclude these modes as the source. The net result of our measurements so far has been to bring the theoretical value slightly closer to the data and reduce the uncertainty by about 30%, such that the significance of the difference is unchanged.

References

- [1] J.P. Lees, et al. (*BABAR* Collaboration), arXiv:1306.3600 [hep-ex], submitted to Phys. Rev. D.
- [2] J.P. Lees, et al. (*BABAR* Collaboration), Phys. Rev. D **86**, 012008 (2012).
- [3] J.P. Lees, et al. (*BABAR* Collaboration), Phys. Rev. D **85**, 112009 (2012).
- [4] B. Aubert et al. (*BABAR* Collaboration), Nucl. Instr. Methods A **479**, 1 (2002); arXiv:1305.3560 [hep-ex], submitted to Nucl. Instr. Methods.
- [5] J.P. Lees, et al. (*BABAR* Collaboration), Phys. Rev. D **86**, 032013 (2012).
- [6] J. Beringer, et al. (Particle Data Group), Phys. Rev. D **86**, 010001 (2012).